Reducing the false alarm rate of a Met Office automatic volcanic eruption detection system

H.A. Watkin, T.R. Scott, I. Macadam, L.C. Radice and D.J. Hoad

June 2003

Abstract

An automatic volcanic eruption detection system was developed by the Met Office and described by Scott et al. (2001). It searched infrared images from Meteosat for characteristic volcanic cloud shapes that passed location, height, and contrast checks. It had a reasonable eruption detection rate, but a false alarm rate that was too high for the system to be of operational use. This paper describes improvements that were made to the system with the aim of reducing the false alarm rate to an acceptable level.

The main changes were to the cloud identification techniques and the cloud checking techniques used in the system. Firstly, the shapes that are searched for in the images were altered so that they better represent the shape that might be expected for volcanic ash clouds given the local meteorological conditions. Secondly, new checks to verify that the cloud had the characteristics of a volcanic eruption cloud were carried out. These included a check that the cloud had not been present upwind of the volcano in a previous image, and that it was not of a similar brightness temperature to other clouds in the area.

The upgraded eruption detection system successfully rules out over 90% of the false alarms when compared to the original system. 12 out of the 18 eruptions in the 1996-2002 sample in the Meteosat field of view are successfully detected. The statistics given in this report will allow the London VAAC to choose a system that best suits their operational requirements. The volcanic eruption detection system should provide a valuable additional tool to the VAAC as they strive to keep aviation informed of the hazards of volcanic ash.

Document review history

Date	Version	Action/comments	Approval
04/06/2003	1	First draft for comments	
20/06/2003	2	Second draft for review	
24/06/2003	3	Third draft incorporating comments	Paul Agnew

CONTENTS

Page

1. Introduction

Ash clouds produced during volcanic eruptions can reach aircraft cruising altitudes and pose a significant hazard for the aviation community. The particles of silicate contained in the clouds can cause erosion of aircraft engine parts, wings and windscreens which can be costly to repair. If the engines are hot enough to melt the silicate then it can accumulate on turbine blades as glass and lead to in-flight engine shutdown. In 1982 a British Airways Boeing 747-200, flying at an altitude of 11,470 metres, flew through a volcanic ash cloud from Mt Galunggung, Indonesia, and lost power to all four engines, which only restarted after a loss of altitude of around 7000 metres. An encounter in 1989, when a KLM 747 flew through an eruption plume from Mt Redoubt in Alaska, prompted the First International Symposium on Volcanic Ash and Aviation Safety, held in Seattle, Washington in July 1991. One of the outcomes of this meeting was the development of nine Volcanic Ash Advisory Centres (VAACs) around the world, each responsible for identifying volcanic ash in their region and providing warnings to airlines of areas that should be avoided.

It is the responsibility of Volcanic Ash Advisory Centres (VAACs) to forecast the movement of volcanic ash clouds at flight cruising levels, but in order to do this they need to know that an eruption has occurred. Notification of an eruption usually comes from eyewitness or pilot reports, or from volcano observatories, but this can be a slow and unreliable process, especially for volcanoes that are isolated either geographically or politically. For instance, although the January 2002 eruption of Mt Nyiragongo, in the Democratic Republic of Congo, was widely reported by the world's media, there is still uncertainty as to when the eruption began.

There is thus a need for a system that can automatically detect volcanic eruption clouds worldwide using satellite images. Its use could allow volcanic ash warnings to be issued to airlines much earlier than if reliance is placed on conventional reporting. Such a system was presented in Scott et al. (2001), but unfortunately had a very high false alarm rate.

The aim of this study was to reduce the false alarm rate of the detection system to a few per day without reducing the probability of detection. This level of false alarms would be acceptable by the London VAAC and would thus allow the system to be made into an operational product.

2. The basic volcanic eruption detection system

The original volcanic eruption detection system was developed by Scott et al. (2001). As that report carries a full description of the methods involved, the theory behind them, and the parameters used by the system, only a summary of the system is provided here.

The system operates by generating plume- and circle-shaped cloud templates (referred to as kernels) for each of the 850, 700, 600, 500, 400, 300, 250, 200 and 150 hPa pressure levels within the *sub-image* (the area inside a ten-pixel radius of the volcano) for each volcano being monitored at each satellite image time. A cloud present in the sub-image must satisfy the following conditions at a certain pressure level in order to be detected:

- When correlated with a plume- or circle-shaped cloud template there is a correlation value $C_{k,l}$ that exceeds the pre-defined correlation threshold C_{crit}, indicating a good match between the template and the cloud. The correlation method used is described in greater detail by Gonzalez and Wintz (1977).

- The coldest brightness temperature within the detected cloud, $T_{k,l}$, falls between T_{below} and T_{above}, where
  - T_{below} is the average of the temperature at that pressure level and the temperature at the level immediately below
  - T_{above} is the average of the temperature at that pressure level and the temperature at the level immediately above.

  The location of $T_{k,l}$ defines the *cloud top location*, $L_{k,l}$
- The distance $R_{k,l}$ between $L_{k,l}$ and the volcano is less than a pre-defined threshold R **or** the perpendicular distance $P_{k,l}$ between $L_{k,l}$ and the downwind direction is less than R.
- $R_{k,l}$ is less than the distance $D(t)$ corresponding to a time t downwind.
- The brightness temperature variance $S^2_{k,l}$ over the cloud is greater than a pre-defined threshold S^2.

The thresholds used by Scott et al. (2001) were C_{crit}=0.8, R=2.5 pixels, D=1.5 hours and S^2=25K^2.

In total the original system was tested on 18 eruptions. This figure includes the 7 eruptions used in Scott et al. (2001) for setting the detection parameters. Of these 18 eruptions, 14 were successfully detected and 4 were not detected.

During the real-time operation of the original detection system for a 35-day period in July-August 2001, monitoring 90 volcanoes in the Meteosat 7 field of view, there were 3363 false alarms or roughly 100 per day. A false alarm is when the system claims to have detects a volcanic eruption cloud, but there was not a volcanic eruption in that area at that time. Given that there were 48 images per day, this means that for every examination of a volcano by the detection system there was on average a 2.4% chance of a false alarm. A similar rate occurred when the system was tested on satellite images from January 2003. This false alarm rate was roughly an order of magnitude too high for the system to be of use to the London VAAC.

3. Strategy for reducing the number of false alarms

A three-stage strategy was developed in order to reduce the number of false alarms:

1. A week's sample of false alarms produced by the original system was collected and the characteristics of this sample investigated. This helped to help find areas on which to focus in order to rule out as many false alarms as possible.
2. Various methods were investigated in order to improve the cloud identification techniques. This mainly focused on improving the modelling of the expected cloud shapes (the circle- and plume-shaped kernels) used to find 'candidate clouds' that have shapes characteristic or volcanic eruption clouds.
3. New cloud checking techniques were developed to validate that a candidate cloud has the temporal and spatial characteristics of a volcanic eruption cloud rather than a meteorological cloud.

Only those ideas that were implemented into the final system are discussed in sections 3.2 and 3.3. Details of other cloud identification and checking techniques that were investigated but not implemented are contained in Appendix D.

3.1 False alarms characteristics of the original system

The original system was run for a seven-day period from 2-8 January 2003, producing a total of 682 false alarms. Figure 3.1.1 shows that there is a large variation in the number of false

alarms per day in the sample period. The number of false alarms produced at each time of day showed a much flatter distribution.

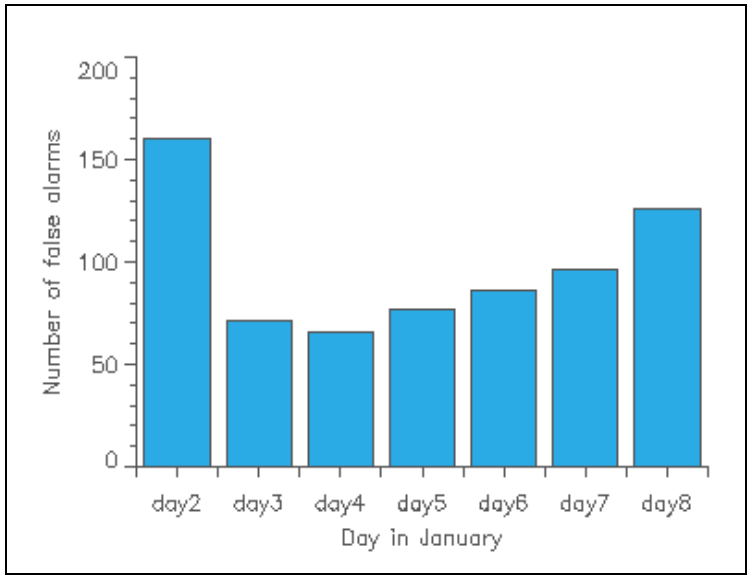

Figure 3.1.1: Number of false alarms produced by the original eruption detection system on each day of the trial period 2-9 January 2003.

Figure 3.1.2 shows the variation in the number of false alarms with each pressure level. The distribution is approximately normal, with detections being most common between 500 and 300hPa. This is to be expected as low altitude clouds of the correct shape will either fail the contrast condition or be obscured by higher clouds, and high altitude clouds with a small distinct shape are rare. Those pressure levels corresponding to flight cruising levels and above are shown by the dotted shading.

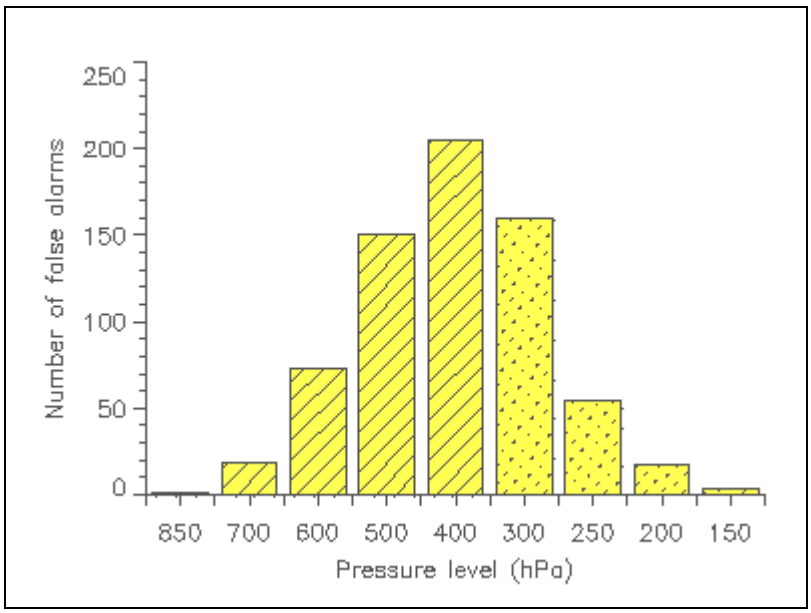

Figure 3.1.2: Number of false alarms detected at each pressure level by the original eruption detection system for the trial period 2-9 January 2003.

Figure 3.1.3 shows the variation of each of the system parameters for the sample of false alarms. In the original system, all correlations of 0.8 and above are accepted as candidate clouds. The top left graph shows that around half of the false alarms fall within 0.80 and

0.85, with the number of false alarms gradually dropping off as the C value increases. The fall with the contrast parameter (S^2) is even more dramatic (top right), with the vast majority of false alarms having S^2 values falling between 25 and 50. This shows that if the C_{crit} or S^2 threshold parameters could be raised even slightly, the reduction in false alarm rate would be significant. The C_{crit} parameter could be raised if the correlation between the expected cloud shapes and the eruption clouds could be increased (see section 3.2). The S parameter could be raised if the system only searched for clouds at higher altitudes which have a greater contrast with their surroundings (see section 5.1). The bottom two graphs show the tests that must be passed in the location test for the cloud to be counted as downwind of the volcano (P<2.5 and D<1.5). The false alarms are nearer to being ruled out the closer to the right of the graph they are. The distribution of P values is fairly even, while most false alarms fall comfortably below the D threshold, indicating that lowering these thresholds would not lead to a substantial reduction of the false alarm rate.

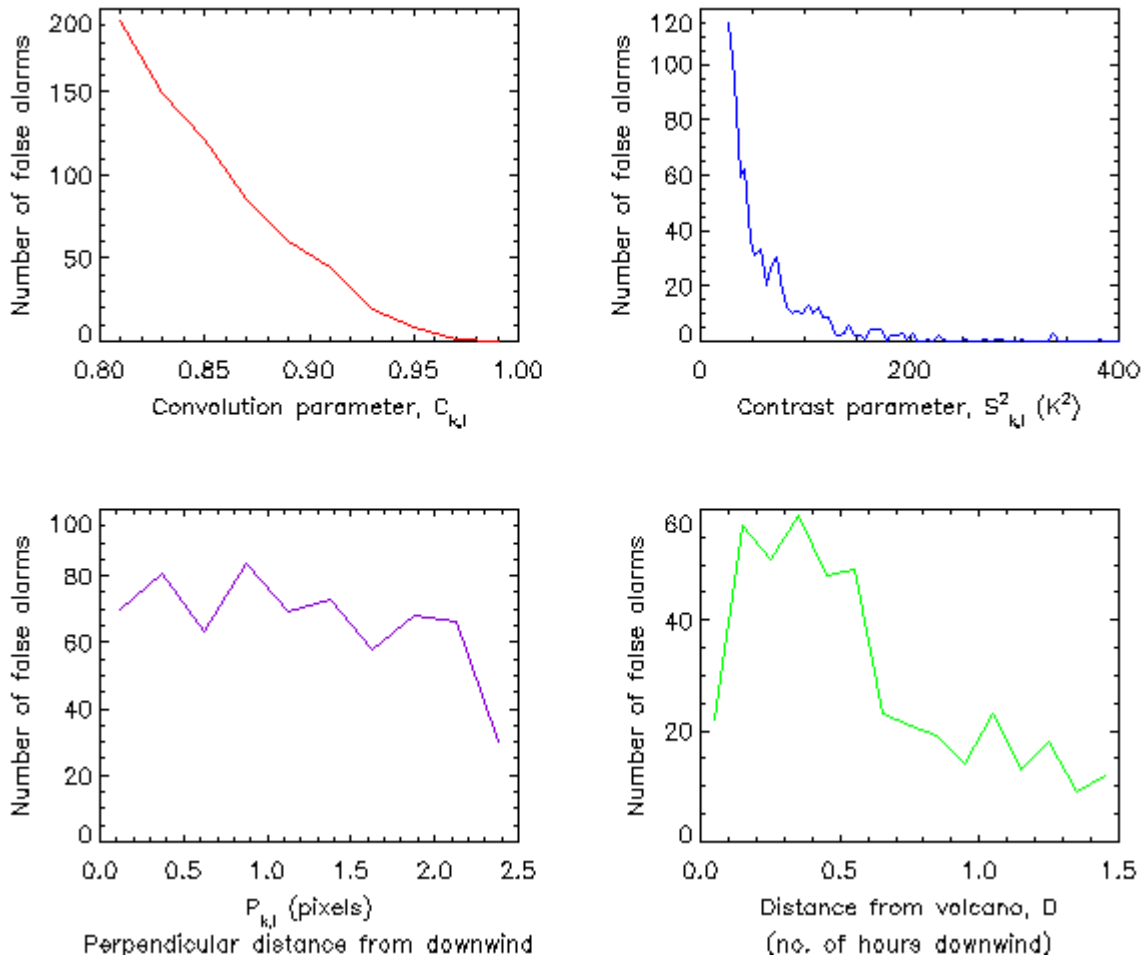

Figure 3.1.3: Histograms showing the variation in each of the parameters for the sample of false alarms produced by the original system.

3.2 Improvements to the expected cloud shape

Two types of kernel were generated in the original system and matched with the satellite image using pattern recognition techniques: a circular kernel and a plume-shaped kernel. The circular kernel had a constant radius of 1.75 pixels and the plume kernel a constant angular width of 40°. In reality both the radius of the circular cloud and the angle of the plume vary. One option was to allow these values to vary and to match a number of kernels at each height. However, this would increase the false alarm rate, and thus effort was focused on creating kernels that are specific to the height in question and the forecast

weather conditions. In doing this, the aim was to increase the correlation parameter ($C_{k,l}$) for real eruptions, allowing the correlation threshold to be raised and more false alarms to be ruled out. The detailed method for creating the kernel is described by Scott et al. (2001).

Circular kernels

Circular clouds are expected:

a) if the eruption is very strong and the eruption cloud has not been significantly affected by the wind;
b) if the wind is very weak.

The radius of the plume depends on time since eruption, eruption height, eruption strength, and whether or not it has reached the Neutral Buoyancy Height (NBH), where it begins to spread out sideways to form an umbrella cloud.

Increasing radius with height

As a plume rises and the density of the atmosphere decreases, the plume expands. Thus the radius of the plume increases with height even before the NBH is reached. After the NBH has been reached the column spreads out to form an umbrella cloud. The rate and extent of this spreading increases with eruption strength. Stronger eruptions have a higher NBH. Thus, whether or not the column has reached its NBH, *in general* the higher the volcanic cloud is the greater its radius will be. Thus, in the new upgraded system, for each height at which a kernel is created a different radius of circle was used, with this radius increasing linearly with height in hPa, from 0.75 pixels at 850hPa to 1.75 pixels at 150 hPa. These values were chosen by testing the kernels on past circular-shaped eruption clouds.

Projecting the circle kernel

The method of Scott et al. (2001) used the same circular cloud shape for all volcanoes regardless of their position on the satellite image. This may have adversely affected the detection of volcanic eruptions with a large angle of view from the satellite, such as the Caribbean and Icelandic volcanoes, where the spatial resolution of pixels is substantially lower than at the sub-satellite point. A new method for creating the circular cloud kernel was developed to incorporate projection effects. In this method an array of digital coordinates centred on the volcano location was created which was then translated into an array of latitudes and longitudes. These geographical coordinates were then converted into the latitudes and longitudes for a rotated pole grid, centred on (0,0). From this the angular distance from each grid point to the centre was calculated. Those points with angular distances less than the assumed cloud radius could then be assigned as part of the cloud in the kernel.

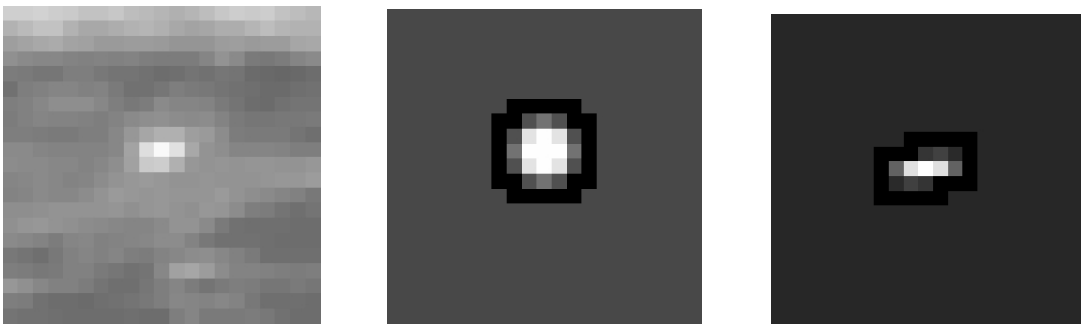

Figure 3.2.1: Infrared image of the Grimsvötn area at 1030Z on 30th September 1996 (left), and the old (centre) and new (right) circular kernel cloud shapes. The new kernel is clearly a better fit with the observed cloud.

One eruption this method proved effective for was the October 1996 eruption of Grimsvötn, situated beneath Iceland's Vatnajökull glacier. This eruption began on 30 September 1996.

At 1000Z on 2 October the eruption cloud broke through the glacier but it was not at that stage visible on Meteosat images. The following day an eruption column reaching 10 km was seen by a ground observer at 1010Z (Michigan Technical University, 1996). This eruption column was visible on the 1030Z satellite image (figure 3.2.1, left). The original detection system detected a circle-shaped cloud on this image at 500 hPa (centre), with a correlation value $C_{k,l}$ of 0.84. With the new method for creating circular kernels (right) a circular cloud was detected with an improved correlation value of 0.86.

Downwind plume kernels

In the Scott et al. (2001) system a triangular shape with an angular width of 40° in the downwind direction was used. In reality this angular width varies between eruptions and with wind speed. A triangular shape also oversimplifies the actual volcanic cloud shape, which tends to be more parabolic.

Rose et al. (2001) and Bursik et al. (1992) give an equation (also given in Sparks et al., 1997) for the parabolic plume shape produced by a strong eruption. This equation assumes that plume spreading takes place as an intrusive gravity current while downwind advection is occurring, and produces a cloud width which is proportional to the square root of the downwind distance and inversely proportional to the wind speed:

$$y(\max) = U^{-1}\left(2\lambda NQx\right)^{1/2} \tag{1}$$

where y(max) is maximum cloud width for a downwind distance of x, U is windspeed at the cloud height, λ is a parameter (~1) that depends on flow geometry, N is the Brunt-Vaisala frequency of the atmosphere, and Q is the volumetric flux of material. For strong eruptions, Q is related to column height:

$$Q = \left(Height / 0.287\right)^{5.3} \tag{2}$$

In weaker eruptions the height that a plume reaches is controlled by the wind, temperature and humidity profiles (Graf et al., 1999; Bursik, 2001; Simpson et al., 2000). Thus height cannot be used alone to calculate Q. In addition, spreading in weaker eruptions is largely by turbulent diffusion, rather than as a gravity current. The following equation is given in Sparks et al. (1997), and produces a cloud width which is proportional to the square root of the downwind distance and inversely proportional to the square root of the wind speed:

$$y = 4\sqrt{\frac{k_h x}{w}} + b_0 \tag{3}$$

where y is cloud width, k_h is atmospheric horizontal eddy diffusivity, w is wind speed and b_0 is initial plume radius.

Sparks and Ernst (2002) suggested that the two equations above could be simplified into the following equation, negating the need to calculate k_h, which is difficult outside the boundary layer:

$$y = a\frac{x^{1/2}}{u^n} + b \tag{4}$$

where y is cloud width for a downwind distance of x, u is the wind speed, a is a parameter representing plume spreading and b represents initial plume radius.

Best-fit parameters for a and b for each height were decided following the measurement of plume dimensions in past eruptions, and the value of 'n' was set to 0.5. Thus the final equation used in the system is similar to the turbulent diffusion equation (3). A value of 200 for parameter 'a' was found to be the optimum value for eruptions at all heights. The value of 'b' used at each height are given in table 3.2.1.

Pressure level	850	700	600	500	400	300	250	200	150
b (m)	2500	2750	3000	3250	3500	3750	4000	4250	4500

Table 3.2.1: Best fit values of the b parameter derived from measurements of past eruptions.

Eruptions that rise steadily through the troposphere are susceptible to wind shear, which can create a wider-shaped plume. Thus if directional wind shear was present, the value of a was increased, by up to 25%, depending on the severity of the shear.

The downwind plume-shaped kernel is thus dependent not only on wind direction, but also on wind speed and the assumed height of the cloud. The initial width of the parabolic plume shape used in the kernel increases with the assumed plume height, while the downwind plume shape gets narrower as the wind speed increases, as downwind advection begins to dominate over the horizontal plume spreading (as a gravity current or due to diffusion).

An example of the new plume-shaped kernel is shown for the February 2000 eruption of Hekla in figure 3.2.2. The original detection system detected a plume-shaped cloud on the 1900Z image (left) at 300 hPa, with a correlation value $C_{k,l}$ of 0.89 (centre). With the new method for creating plume kernels (right), the eruption was detected with a correlation value of 0.92.

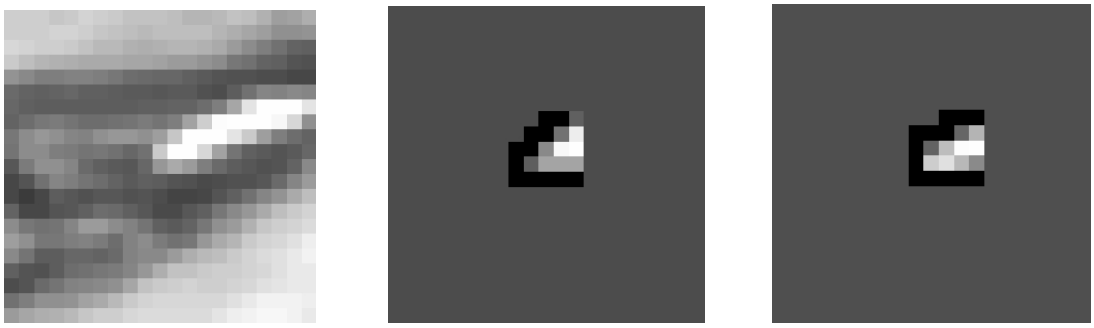

Figure 3.2.2: Infrared sub-image of the Hekla area at 1900Z on 26th February 2000 (left), and the old (centre) and new (right) plume kernel cloud shapes.

Ideally the plume kernels would also be projected to represent the angle of view of the satellite at the volcano in question. This should be incorporated into any future development of the system.

Implementing the new kernels

The new kernel shapes were assessed by running the system using the images for several eruption cases. These images produce false alarms for some of the other volcanoes in the Meteosat field of view. On average, the new shapes eliminated about 35% of false alarms produced using the original shapes, when the correlation threshold of C_{crit}=0.80 used by Scott et al. (2001) was applied.

However, the correlation value ($C_{k,l}$) was raised for several of the eruptions in our sample, indicating a better shape-match between the expected cloud shapes and the volcanic eruption clouds in question. Crucially, several eruptions that had previously been detected with correlation values between 0.80 and 0.84 were now detected with $C_{k,l}$ values of above 0.84. This meant that in the new detection system the C_{crit} threshold applied could be raised from 0.80 to 0.84, ruling out around 50% of the remaining false alarms. Thus in total, using the new shapes and raising the C_{crit} threshold rules out around two thirds of the false alarms.

Three eruptions that were previously detected by the plume shape are now detected by circle kernels, which given the documentary and visual evidence should indeed fit the eruption cloud better. In addition to being of scientific value, this gives two additional benefits:

1. A wind speed condition can be implemented. A plume-shaped kernel is searched for only if the wind speed is greater than 3m/s, because when the wind speed is very low a circular shaped volcanic cloud would be expected. When this condition was tested, around 3% of the original sample of false alarms were ruled out.

2. Any eruptions with correlation locations that are greater than the threshold distance (R) upwind can be ruled out as false alarms. In the original detection system, the eruption of Etna on 23/01/1999 was detected by a plume kernel with an upwind correlation location. It was retained as a detection because the cloud top location $L_{k,l}$ was within distance R of the volcano. This loophole can now be closed because this eruption is now detected with the new circle kernel. Tests showed that this condition eliminates around 28% of the false alarms.

3.3 Additional cloud checking techniques

Temporal check

If a candidate cloud is actually a meteorological cloud, it can often be seen upwind of the volcano in a previous image. For example, see figure 3.3.1. On this occasion, the eruption detection system identified a candidate cloud over Mount Meru in Tanzania. However, the candidate cloud can be seen upwind of Mount Meru in the previous image half an hour earlier.

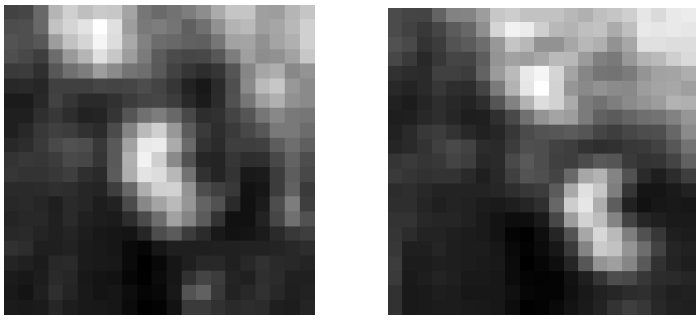

Figure 3.3.1: a) Candidate cloud detected over Mount Meru, at 0900Z on 17/1/2002. b) The same cloud can be seen upwind of Mount Meru half an hour before detection. (The projected wind angle was 147.3°.)

This check is implemented by estimating the position of the candidate cloud in the previous image using the wind vector, checking that this is upwind of the volcano, then searching for the candidate cloud in the previous image using the correlation technique at this approximate position. If the estimated cloud position in the previous image is not upwind of

the volcano, then the position of the cloud in the image before that is calculated. If this is not upwind of the volcano either, the check is not performed.

This check was assessed by running the system using the images for all the eruption cases. On average, it eliminated about 18% of false alarms. However, the check eliminated two eruptions:

- The detection of Soufrière Hills at 0830Z, 6/8/1997. In this case there were bands of meteorological cloud present close to the volcano (see Appendix B).
- The detection of Nyamuragira at 2100Z, 27/07/2002. This eruption was originally detected at 500 hPa following an eruption 18 hours before. There were also some meteorological clouds in the vicinity at the time of the detection at about the same height (see Appendix B).

Grey level check

A candidate eruption cloud is more likely to be a real eruption if there are no other clouds in the vicinity at the same height, because if other meteorological clouds are nearby at the same height it is likely that the candidate cloud is also a meteorological cloud. For example, see the image for the eruption of Etna at 0630Z on 23/01/1999 in figure 3.3.2.

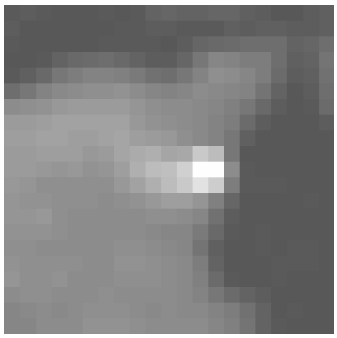

Figure 3.3.2: Candidate cloud detected over Etna at 0630Z on 23/01/1999. The eruption cloud and the outline of the Sicilian coast can clearly be seen but there are no other clouds at the same height in the vicinity. Thus this candidate cloud is likely to be an eruption cloud and easily passes the grey level check

This check was implemented by examining the grey levels in the sub-image (i.e. over an area of 21 x 21 pixels) away from the candidate cloud, or away from the downwind area of a plume kernel. The numbers of pixels having a grey level between the coldest and the next-coldest grey levels in the candidate cloud are counted. If this number is less than a threshold of 10 pixels, the candidate cloud is deemed to have passed this test. This threshold was set so that none of the originally detected eruptions were eliminated.

This check was then assessed by running the system using the images for the eruption cases. This trial indicated that the test eliminated about 40% of false alarms. This check will not rule out isolated orographic clouds positioned over the volcano.

Sudden appearance check

A candidate eruption is more likely to be a real eruption if the cloud has suddenly appeared on the satellite image. If there is no cloud with similar grey levels in the satellite image an hour before detection, the candidate cloud is likely to be a real eruption. For example, see the sequence of images for the eruption of Nyiragongo on 17 January 2002 shown in figure 3.3.3.

To test this, the coldest value and next-coldest value in the candidate cloud is determined. Then a 14 x 14 pixel area centred on the volcano from the image taken an hour beforehand is examined and the number of pixels with values between the coldest and next-coldest values is calculated. If this number is less than a threshold of 10 pixels, the candidate cloud is considered to have passed this check. Again, this threshold was set so that all of the originally detected eruptions passed this check.

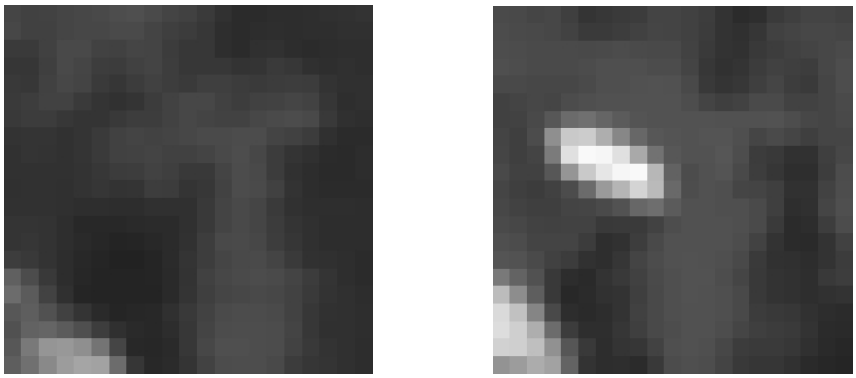

Figure 3.3.3: Sequence of images illustrating the sudden appearance of the cloud for the eruption of Nyiragongo, 17/01/2002: a) Nyiragongo, 0700Z; b) Nyiragongo, 0730Z

This check was trialled by running the system with the images for the eruption cases. This trial indicated that the check eliminated about 35% of false alarms. However, a large portion of these were also eliminated in the grey level check trial.

Convective cloud check

Many of the false alarms from the original system may have been caused by convective clouds with similar shapes to volcanic eruption clouds. The Met Office Unified Model produces a forecast of the expected height (in hPa) of any convective cloud in the area. If this height is close to the height of the candidate cloud, then it is very likely that this cloud is in fact convective and not volcanic in origin. Thus a test was developed to rule out as a false alarm any candidate cloud with a height within 100hPa of the convective cloud top. A trial of this check using the images for the eruption cases showed that it ruled out approximately 8% of false alarms and none of the eruptions.

4. Performance of the updated volcanic eruption detection system

Following the trials discussed above, the new kernels, and the temporal, grey level, sudden appearance and convective cloud checks were incorporated into the final updated detection system. The new system was run for the 18 eruptions in the eruption archive to calculate a final probability of detection. It was also run from 10-15 January 2003 in order to calculate its false alarm rate.

4.1 Effectiveness of detecting eruptions

An archive of images covering volcanic eruptions in the Meteosat 7 field of view has been accumulated since 1996. To be considered for inclusion in the archive, reports had to specify a specific date and time for the eruption, and state that it had produced an ash cloud that had reached Flight Level 100 (FL100) or above. In addition, the eruption cloud had to be visible by eye in the Meteosat infrared image. It should be noted that if eruptions were included in the archive that did not fit these criteria, the detection rate would have been

correspondingly lower. Of the 18 eruptions in the archive, the following results were found using the new updated system:

- 12 were successfully detected by the system, with $C_{k,l}$ values varying between 0.84 and 0.94. Images of those eruptions that were detected are contained in Appendix A.
- 6 were missed by the system (images of these eruptions are contained in Appendix B). Of these 6, 4 were also missed by the old system, due to very low contrast values, or problems in the wind direction. However, 2 eruptions that were previously detected by the old system are now ruled out. The eruption of Soufrière Hills in Montserrat on 06/08/1997 is no longer detected by the new kernel shapes, probably because of the low contrast with its surroundings. Even if it had been detected it would have been ruled out by the temporal check due to the lines of meteorological cloud in the surrounding area. The eruption of Nyamuragira on 27/07/02 is also eliminated by the temporal check due to other meteorological cloud in the area.

4.2 New false alarm rate

The eruption detection system was tested on two samples of data: 10-15 January 2003 and 20-24 July 2001. The results from this period are shown in tabular form in Appendix C.

In the week 10-16 January, the updated eruption detection system detected 72 false alarms when monitoring 90 volcanoes. This represents a 0.3% chance of the upgraded system producing a false alarm each time is checks a volcano. When compared to the 2.5% chance in the original system this represents around an 88% reduction in the false alarm rate.

The system was also run for a sample of images from July 2001 in order to check that the January week had been representative of the year-round false alarm rate. In fact it was found that for this sample of data, the eruption detection system had only a 0.1% chance of producing a false alarm per volcano per image. This represented a 95% reduction in the number of false alarms when compared to the original system. Thus it appears that the false alarm rate has some temporal and possibly seasonal variation. For example, the volcanic regions covered may be more prone to meteorological cloud at certain times of the year, and thus the system is more likely to produce false alarms at these times. Due to these factors it may be misleading to give one figure for the false alarm rate, but in the absence of more detailed statistics, the average false alarm rate is taken to be the mean of the two samples, i.e. 0.002 false alarms per volcano monitored per image.

5. Discussion

5.1 Operational considerations

The false alarm results presented in section 4 will allow the London VAAC to choose the eruption detection system which best suits their user requirements. For example, if the maximum number of false alarms that they could cope with is 5 a day, then the system could monitor around 52 volcanoes of their choice, assuming the average false alarm rate found in section 4.2. However, if they in fact were only interested in monitoring the Icelandic volcanoes, then the system would produce just one or two false alarms per day.

A further consideration is at which heights the VAAC would want the eruption detection system to search for volcanic clouds. Currently the system looks for ash clouds from 850hPa (FL50) and above. If the VAAC only wanted the eruption detection system to search for clouds at flight cruising levels, it could be set to search only at 300hPa (FL300) and above. Referring back to figure 3.1.2 it is clear that this would immediately rule out over half of the false alarms (those shown by solid line shading). In addition, eruptions at these heights have

higher contrast values, so the contrast parameter (S^2) could be raised from 25 to 50. Due to the steep drop off in S^2 values for false alarms (as shown on figure 3.1.3), this would rule out a further large portion of false alarms, as shown by the final column of the tables in Appendix C. Thus the London VAAC could monitor all Icelandic volcanoes at flight cruising levels and receive a false alarm only about once every three days.

The London VAAC will be able to use the volcanic eruption detection system in combination with the existing AVHRR volcanic ash detection product, described by Watkin (2001). This product displays the brightness temperature difference between two channels, at 10.8 and 12.0 μm, with negative brightness temperature differences being indicative of volcanic ash. An additional "split-window" product will be developed using Meteosat Second Generation (MSG) images later this year, and could provide one way of assessing whether the alert produced by the eruption detection system is an eruption or a false alarm. The two systems may also pick up eruptions that would be missed if only one was available. For example, the brightness temperature difference is reduced in moist atmospheres, or if there is a high proportion of water vapour, liquid water or ice within the volcanic cloud, and thus the eruption detection system may be more reliable under these circumstances. Similarly, the split-window product may pick up eruption clouds with an unexpected shape that would not be detected by the volcanic eruption detection system.

5.2 Suggestions for further work

The project to improve the eruption detection system has met its aim to reduce the false alarm rate to a few per day without substantially reducing the number of eruptions that are successfully detected. Thus a follow-on project will be conducted. Firstly the system will be upgraded to use images from Meteosat Second Generation (MSG), which was launched in August 2002. The MSG camera, called the Spinning Enhanced Visible and Infra-red Imager (SEVIRI), will build up images of the Earth's surface and cloud once every 15 minutes, compared to once every 30 minutes for the camera on Meteosat. The images will also be sharper: at the infrared wavelength used in the detection system, SEVIRI will resolve features 3 km across, compared with 5 km for Meteosat (European Space Agency, 2002). Thus, SEVIRI images will allow the system to provide more timely warnings and should lead to improvements in the shape-matching. Secondly, the upgraded system will be operationally implemented on the Met Office's Satellite Processing System to allow it to be used by the London VAAC.

Several other ideas for future work also stem from this project:

- The system should be tested on any new eruptions that occur in the Meteosat field of view to continue to build up the probability of detection results.
- The plume kernels should ideally be reprojected in a similar way to the circle kernels to take into account the angle of view of the satellite at each volcano.
- It may be possible to implement an orographic cloud test in addition to the convective cloud check. This would use meteorological data in combination with the altitude of the volcano to calculate if convection would be initiated when a parcel of air is lifted over the volcano. If the predicted height of the orographic cloud was close to that of the candidate cloud, the cloud could then be eliminated as a false alarm.
- The height test could be improved to lessen the risk of an eruption being missed in cases of severe directional wind shear, or if the eruption is at a large angle of view from the satellite.
- Currently, a candidate cloud needs to pass all the cloud checks to prevent it being ruled out as a false alarm. A different option would be to use each test to provide a assign a 'probability of eruption' value to the candidate cloud. For example, if the shape match has a certain value then what is the probability that the candidate cloud is an eruption rather than a false alarm? Or if the candidate cloud has suddenly appeared in the image

then the probability of an eruption might be quite high. All of these probabilities could be multiplied together to give an overall probability of eruption. A threshold value could then be applied. This reduces the sensitivity of the system to each individual test and should reduce the chance of an real eruption being ruled out without increasing the false alarm rate.
- Geographical studies could be carried out once the system becomes operational. The results could be analysed to see if certain volcanoes or seasons were more likely to produce false alarms.
- The system could be developed to run on other geostationary satellites such as Meteosat 5, GOES and GMS. This would increase the number of eruptions that the detection system could be tested on, due to the increased level of volcanic activity in the areas covered by these satellites.
- Other volcanic ash detection methods, such as the 'split window' channel difference, SO_2 detection, or hot-spot detection methods, will be possible with the additional channels that are available on MSG. These methods could be incorporated into the volcanic eruption detection system, or used in conjunction with the system to rule out false alarms or verify that an eruption cloud is present.

6. Summary and conclusions

This project has upgraded the automatic volcanic eruption detection system developed by Scott et al. (2001). The cloud identification techniques have been improved through creating new circle- and downwind plume-shaped kernels, which are in the shape that would be expected of a volcanic eruption cloud given the height and meteorological conditions in the area. Once a candidate cloud is identified, a number of extra cloud checking techniques have been developed in order to check that it has the characteristics expected from a volcanic eruption cloud. These include:
- a temporal check which classes the cloud as a false alarm if it was present upwind of the volcano in the previous image
- a check that the cloud has suddenly appeared in the area
- a check that there are not other clouds at similar heights in the area
- a check that convective cloud is not forecast at that height

The new cloud identification and cloud checking techniques have succeeded in reducing the number of false alarms by around 92%, when compared to the original system. The system can now monitor around 52 volcanoes to achieve a false alarm rate of around 5 a day, a figure which has previously been thought to be operationally acceptable by the London VAAC (Smith, 2000). The eruption detection system correctly detects 12 out of the 1996-2002 sample of 18 eruptions in the Meteosat field of view. This is only 2 less than were detected by the original detection system. It should be emphasised that the system will struggle to detect an eruption if it is obscured by meteorological cloud or if there is meteorological cloud in the area at a similar height. As the expected cloud shapes were designed using a sample of prior eruptions it is also possible that a future eruption will not fit this pattern and will prove difficult to detect. However, this system is believed to be the only automatic detection system available using shape-matching methods and as such provides a useful additional tool for use by the VAAC.

The statistics shown in this report should allow the London VAAC to choose a system that best suits their operational requirements. For example, if they were satisfied to only look for Icelandic eruption clouds that have reached flight cruising levels, then the false alarm rate could be reduced to just one every few days.

As the false alarm rate is now at an acceptable level for it to be made operational, the eruption detection system will be upgraded to use SEVIRI images from MSG, and then implemented on the Met Office Satellite Processing System. This will allow it to become an operational tool for use by the London VAAC.

Acknowledgements

We would like to thank the following:
- Steve Sparks and Gerald Ernst of the University of Bristol for their advice on equations to use when calculating the expected plume shape.
- Fiona Smith for her assistance with software to calculate solar elevations.
- Bob Lunnon for his encouragement and guidance during the study.

References

Bursik, M. (2001) Effect of wind on the rise height of volcanic plumes. Geophysical research letters, 28(18), 3621-4

Bursik, M.I., Carey, S.N., and Sparks, R.S.J. (1992) A gravity current model for the May 18, 1980 Mount St. Helens plume. Geophysical research letters, 19(16), 1663-6

European Space Agency (2002) Why we need MSG. Webpage: http://www.esa.int/export/esaMI/MSG/ESA5RV66K3D_0.html

Gonzalez, R.C. and Wintz, P. (1977) Digital Image Processing. Addison-Wesley. pp334-337 & 383-385

Francis, P. (1993) Volcanoes: a planetary perspective. Oxford University Press.

Graf, H-F., Herzog, H., Oberhuber, J.M., and Textor, C. (1999) Effect of environmental conditions on volcanic plume rise. Journal of geophysical research, 104(D20), 24309-20

Michigan Technical University (1996) Bárðarbunga/Grimsvötn Volcanoes, Iceland, Report 004. Webpage: http://www.geo.mtu.edu/volcanoes/iceland/vatnajokull/gvn/notice.004.html

Prata, A.J. and Grant, I.F. (2001) Retrieval of microphysical and morphological properties of volcanic ash plumes from satellite data: Application to Mt Ruapehu, New Zealand. Quarterly Journal of the Royal Meteorological Society, 127, 2153-2179

Rose, W.I., Bluth, G.J.S., Schneider, D.J., Ernst, G.G.J., Riley, C.M., Henderson, L.J., and McGimset, R.G. (2001) Observations of volcanic clouds in their first few days of atmospheric residence: the 1992 eruptions of Crater Peak, Mount Spurr Volcano, Alaska. Journal of Geology, 109, 677-94

Sawada, Y. (1987) Study on analyses of volcanic eruptions based on eruption cloud image data obtained by the geostationary meteorological satellite (GMS). Technical Reports of the Meteorological Research Institute, 22

Scott, T.R., McDonald, K.A., and Lunnon, R. W. (2001) Automatic detection of volcanic ash using Meteosat. Forecasting Research Technical Report 369, Met Office

Simpson, J.J, Hufford, G., Pieri, D. and Berg, J. (2000) Failures in detecting volcanic ash from a satellite-based technique. Remote sensing environment, 72, 191-217

Smith, D. (2000) Private communication with Tania Scott

Sonka, M. Hlavac, V and Boyle, R. (1999) Image processing, analysis and machine vision. PWS Publishing. pp190-193

Sparks, R.S.J., Bursik, M.I., Carey, S.N., Gilbert, J.S., Glaze, L.S., Sigurdsson, H., and Woods, A.W. (1997) Volcanic plumes. John Wiley and Sons

Sparks, R.S.J. and Ernst, G.G.J. (2002) Private communication

Watkin, S. (2001) A description of an AVHRR volcanic ash detection product and examples of its application. Forecasting Research Technical Report 358, Met Office

Appendix A: Eruptions detected by the eruption detection system

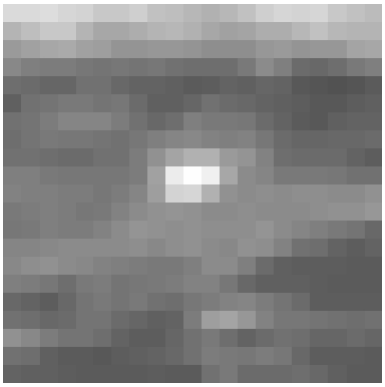

Grimsvötn 03/10/96

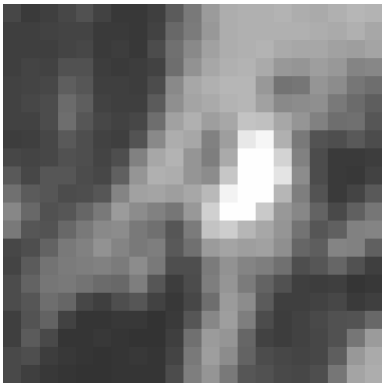

Montserrat 05/08/97

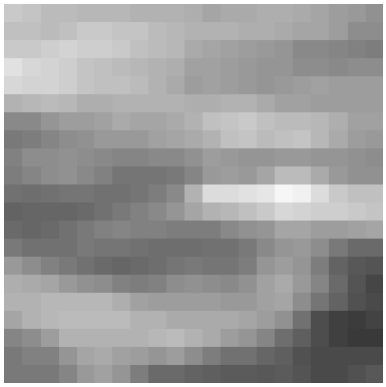

Grimsvötn 18/12/98

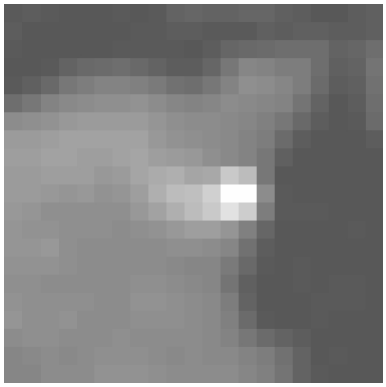

Etna 23/01/99

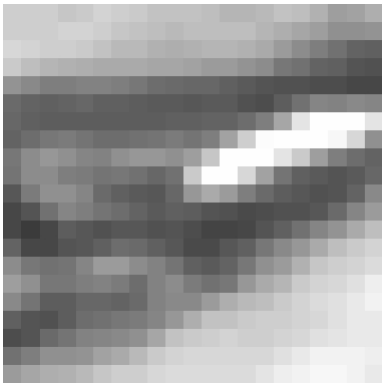

Hekla 26/02/00

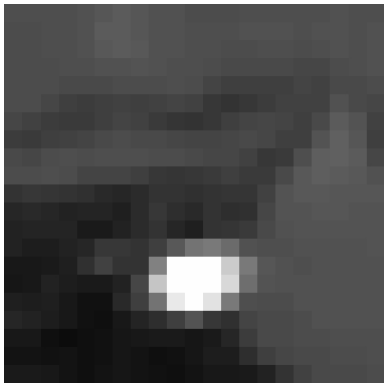

Etna 01/06/00 (am)

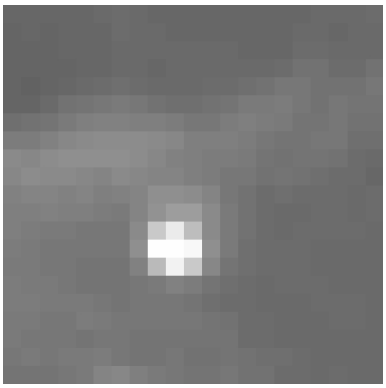

Etna 01/06/00 (pm)

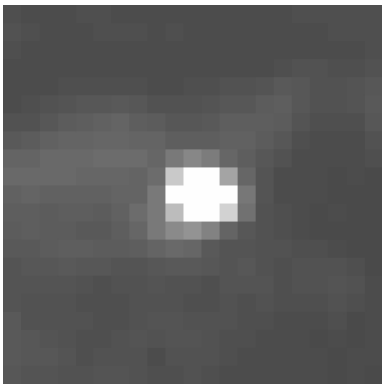

Etna 05/06/00

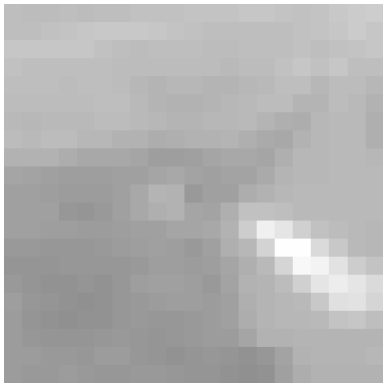

Etna 28/08/00

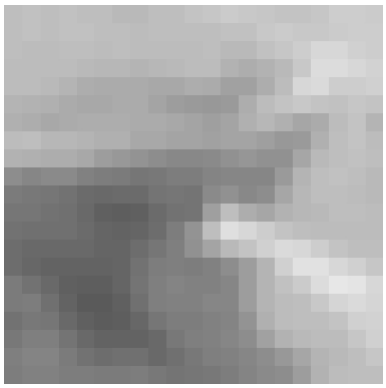

Etna 21/07/01

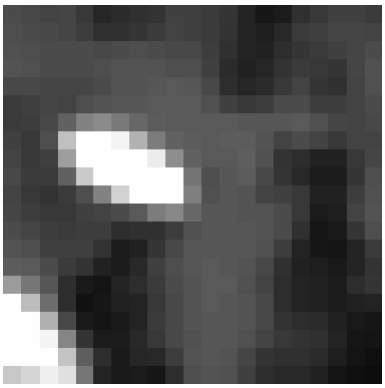

Nyiragongo 17/01/02

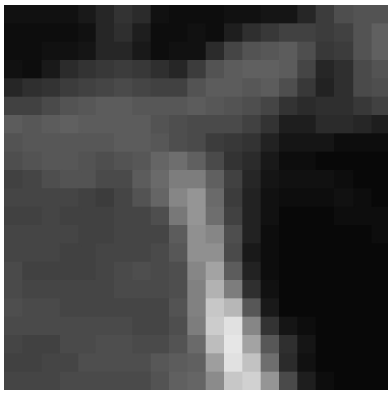

Etna 27/10/02

Appendix B: Eruptions missed by the eruption detection system

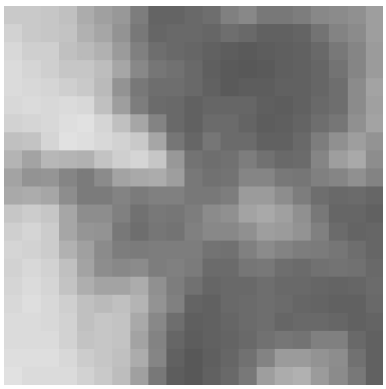

Nyamuragira 04/12/96

Not detected by old or new system. Kernel does not match plume well and there is a low contrast value.

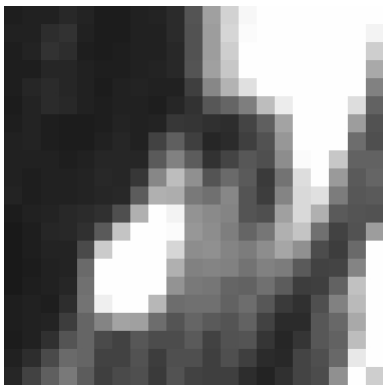

Montserrat 25/06/97

Not detected by either system because plume is spreading in a different direction to the forecast wind speed.

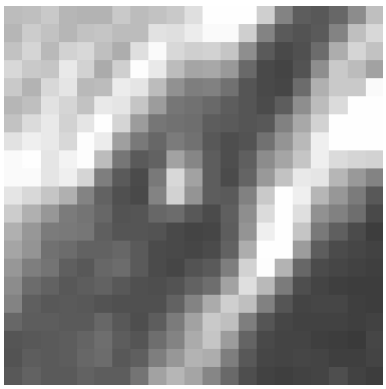

Montserrat 06/08/97

Detected by plume kernel in old system. Not detected by new circle or plume kernels and also ruled out by temporal check

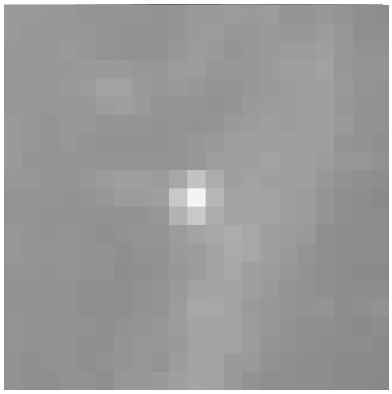

Montserrat 04/08/01

Not detected by either system due to the contrast parameter being below the required threshold.

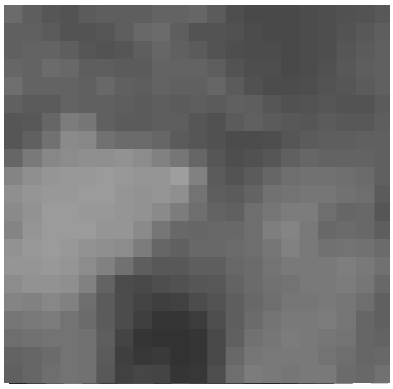

Nyamuragira 25/07/02

Not detected by either system. The shape is not distinct and has a low contrast.

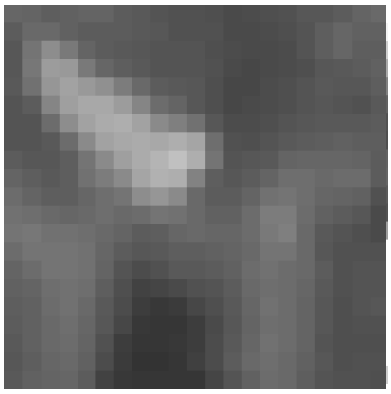

Nyamuragira 27/07/02

Detected by old system. Is ruled out by the temporal check in the new system.

Appendix C: Statistics to compare the false alarm rates of the old and the new eruption detection systems

January 2003 results	Old system (2-8 Jan)	New system (10-15 Jan)	New system above 300hPa only (with higher contrast parameter)
Number of false alarms in a week (monitoring 90 volcanoes)	682	72	15
Number of valid images	300	269	269
False alarm rate per volcano per image	0.0253	0.0030	0.0006
Percentage of false alarms that have been ruled out compared to old system	0.00	88.23	97.55
Number of volcanoes monitored to get false alarm rate of 5/day	4.12	35.03	168.13
False alarm rate per day when only Icelandic volcanoes are monitored	18.19	2.14	0.45

20-24 July 2001	Old system	New system	New system above 300hPa only (with higher contrast parameter)
Number of false alarms in a week (monitoring 90 volcanoes)	350	18	7
Number of valid images	169	169	169
False alarm rate per volcano per image	0.0230	0.0012	0.0005
Percentage of false alarms that have been ruled out compared to old system	0.00	94.86	98.00
Number of volcanoes monitored to get False alarm rate of 5/day	4.53	88.02	226.34
False alarm rate per day when only Icelandic volcanoes are monitored	16.57	0.85	0.33

Average results	Old system	New system (c>0.84)	New system above 300hPa only (with higher contrast parameter)
False alarm rate per volcano per image	0.0241	0.0021	0.0005
Percentage of false alarms that have been ruled out compared to old system	0.00	91.39	97.76
Number of volcanoes monitored to get False alarm rate of 5/day	4.32	50.11	192.94
False alarm rate per day when only Icelandic volcanoes are monitored	17.38	1.50	0.39

Appendix D: Other ideas which were not included in the final system

Reflectivity check

A reflectivity check that used visible satellite images to check the reflective properties of the upper surfaces of candidate clouds was trialled but not included in the final version of the detection system. The check was based on the fact that the reflective properties of volcanic ash clouds are different from those of meteorological clouds in the visible waveband (Sawada, 1987; Prata and Grant, 2001). A "reflectivity" for a cloud appearing in a satellite image, defined as the proportion of visible radiation incident on the upper surface of the cloud reflected towards the viewing satellite, could be estimated from the brightness of a cloud pixel in the image if the following assumptions were made:

- The cloud covers at least the entire pixel in the image and is sufficiently opaque for the brightness of the pixel not to be affected by the nature of the surface underlying the cloud.
- The sun is the only source of illumination for the upper surface of the cloud. This assumption is not valid when the sun is low in the sky as viewed from the cloud because the proportion of direct solar illumination to illumination by radiation scattered by the atmosphere is small under these circumstances.
- Solar radiation travelling from the sun to the cloud is not attenuated or enhanced by atmospheric absorption, scattering or emission. This assumption is not good when the sun is low in the sky as viewed from the cloud because the atmospheric path length between the sun and cloud is great under these circumstances.
- Reflected radiation travelling from the cloud to the satellite is not attenuated or enhanced by atmospheric absorption, scattering or emission. This assumption is not valid when the satellite is low in the sky as viewed from the cloud because the atmospheric path length between the cloud and satellite is great under these circumstances.
- In a transparent atmosphere the reflectivity of the cloud would be independent of the geometrical arrangement of the sun, cloud and satellite.

Software was added to the detection system to estimate the reflectivities of the upper surfaces of any volcanic eruption clouds detected. The system was then run for an archive of eruption clouds. The resulting reflectivity estimates were used to estimate an upper limit to the reflectivity of the upper surfaces of eruption clouds. This was done by assuming that the reflectivity estimates constituted a sample from a normally distributed population of eruption cloud reflectivities. The reflectivity limit was chosen such that 97.5% of ash cloud upper surface reflectivities would be less than the limit. A reflectivity limit, *RL*, of 0.3 was calculated from estimates of the mean, μ, and standard deviation, σ, of the normally distributed population thus:

$$RL = \mu + 2\sigma \tag{5}$$

By identifying clouds with upper surfaces more reflective than this limit as meteorological clouds, it was hoped that the system could make use of this information to reduce the false alarm rate. Unfortunately only six of the archived eruption clouds were detected when the sun was sufficiently high in the sky for a reflectivity estimate to be made. Nonetheless the reflectivity check was trialled in the system with a reflectivity limit of 0.3 for volcanic eruption clouds.

The system was run with the check for a trial week during January 2003. It was found that the check did not contribute significantly to the reduction in false alarm rate exhibited by the system for this trial period. Furthermore it was thought unlikely that the handful of

reflectivity estimates used to calculate the reflectivity limit constituted a representative sample of the reflectivities of the upper surfaces of all volcanic eruption clouds. Hence it was deemed possible that the limit of 0.3 was too low, and that if the final system were to include a reflectivity check that used this limit then it might mistake genuine eruption clouds for meteorological clouds in the future. For these reasons the reflectivity check was not included in the final system.

Using an alternative matching method

The original detection system used a correlation technique to find candidate eruption clouds in an image. This method determines how well a plume or circle kernel matches to a small part of the image. The correlation method used is described in greater detail by Gonzalez and Wintz (1977), and its use in the detection system by Scott et al. (2001).

A different approach to determining how well a candidate cloud matched with a kernel was investigated. The matching method investigated was proposed by Sonka et al. (1997) (their Equation 5.39 and related 5.40), and involves testing the correlation of both the brightness and shape of the candidate cloud (the correlation method used in the original system only tested cloud shape). However, the matching method was defined so that the correlation value was inversely proportional to the difference between the kernel and the image. The matching method was also sensitive to errors in both the brightness and shape. For these reasons, a very low correlation threshold (i.e about 0.05) had to be set for any of the eruptions to be detected. Consequently, more false alarms were identified by the detection system. For this reason this alternative shape-matching technique was not included in the updated detection system.

Cloud-top temperature structure check

It was thought that the cloud-top temperature structures of volcanic eruption clouds and meteorological clouds may differ such that the structure could be used to help rule out false alarms. The structure of volcanic plume-top temperature will vary depending on the strength of the eruption. Strong plumes would tend to show a warmer cloud top further from the volcano, because nearer the volcano the eruption plume exceeds its neutral buoyancy height due to momentum, before spreading out at the NBH. An example of this pattern was shown in the eruption cloud profiles plotted by Sawada (1987) for the Pagan and Una Una eruptions. Weaker sustained eruptions, which gradually rise up through the troposphere, may show a different pattern, getting colder further from the volcano. Unfortunately, the relatively low resolution of the Meteosat infrared images meant that any differences in the cloud top temperature signal of meteorological clouds and volcanic ash clouds were difficult to distinguish and thus the check could not be developed.